Chinese Chemical Letters 32 (2021) 1403–1406

Contents lists available at ScienceDirect

Chinese Chemical Letters

journal homepage: www.elsevier.com/locate/cclet

Communication

Mechanism of the Ir/Pd catalyzed photocarboxylation of aryl halides

Ying Lv[a], Bing Wang[b,*], Haizhu Yu[a,*]

[a] Department of Chemistry and Centre for Atomic Engineering of Advanced Materials, Anhui University, Hefei 230601, China
[b] Department of Chemistry, University of Science and Technology of China, Hefei 230026, China

ARTICLE INFO

Article history:
Received 18 August 2020
Received in revised form 15 September 2020
Accepted 24 September 2020
Available online 25 September 2020

Keywords:
Carboxylation
Pd-catalysis
DFT
Charge state
Mechanism

ABSTRACT

The recent Ir/Pd co-catalyzed photo carboxylation of aromatic halides with CO_2 has shown high efficiency and excellent functional group tolerance for preparing aromatic carboxylic acids and esters. With the aid of density functional theory (DFT) calculations, the carboxylation starts with two parallel steps, *i.e.*, oxidative addition of aromatic halides on Pd^0 and reductive quenching of the photocatalyst $Ir(ppy)_2(dtbpy)^+$ with amine. Thereafter, a successive oxidation of Pd^{II} with the amine radical (generated by the reaction of cationic radical amine and Cs_2CO_3) and Ir^{II} species occurs to generate Pd^0, from which the carboxylation occurs easily *via* a coordination, Pd-C insertion step. The release of the carboxylate product then regenerates the catalyst.

As an abundant, readily-available, green and renewable C1 block, CO_2 has recently attracted increasing research interest [1–12]. The carboxylation of organometallic reagents (such as Grignard reagent and organic lithium reagent) with CO_2 has been reported for decades [13–16]. Despite the great success, these reactions always suffer from the drawbacks such as poor selectivity and harsh reaction conditions (sensitive to water and oxygen). With the development of transition metal catalysts (such as Pd, Ni and Co complexes), highly selective carboxylation with CO_2 have been reported [17–19], using the relatively mild metal/metalloid reagents, such as organotin [20–23], organozinc [24,25] and organoboron [26–32], as substrates.

A breakthrough on direct carboxylation of aromatic halides with CO_2 under mild conditions (40 °C) was recently reported by Martin and co-workers, using Pd/*t*BuXPhos (*t*BuXPhos = 2-di-*tert*-butyl(2′,4′,6′-triisopropyl-[1,1′-biphenyl]-2-yl)phosphine) as the catalyst (Scheme 1a) [33]. Thereafter, a variety of transition metal (such as Ni, Cu) catalysis has been developed, and greatly expands the functional group tolerance of the carboxylation [34–36]. Nevertheless, the used metal reducing agents, such as Et_2Zn and Zn/Mn powder, result in the necessity for post treatment of the metal wastes.

To improve the robustness of the carboxylation reactions, chemists recently developed a series of novel photocarboxylation reactions. For example, Iwasawa and co-workers recently reported the dehalogenation-carboxylation of aromatic halides with the combination of the photocatalyst $Ir(ppy)_2(dtbpy)(PF_6)$ (ppy: 2-phenylpyridine; dtbpy: 4,4′-di-*tert*-butyl-2,2′-dipyridyl) and the transition metal catalyst $Pd(OAc)_2$ (Scheme 1b) [37], in the presence of the additive *N,N*-diisopropyl ethylamine and PhXPhos/*t*BuXphos (PhXPhos: 2-diphenyl(2′,4′,6′-triisopropyl-[1,1′-biphenyl]-2-yl)phosphine). The carboxylation has shown excellent functional group tolerance, and gave the corresponding methyl ester derivatives (after the methyl esterification) in good yields.

The preliminary mechanistic probes by Iwasawa *et al.* suggests a catalytic cycle involving the reduction ($Pd(OAc)_2 \rightarrow Pd^0$), oxidative addition (of aromatic halide), carboxylation, dehalogenation and catalyst-regeneration steps [37]. Albeit the reasonability of the proposed mechanism, some details remain to be clarified. For example, the direct reaction of Pd^{II} with CO_2, or a prior reduction of Pd^{II} to Pd^I or Pd^0 over the carboxylation are all possible (Scheme 2). In other words, the accurate valent state and structure of the precursor before the carboxylation step are still unknown. Meanwhile, the quenching mode of the photocatalyst (oxidative/reductive quenching) and how the photocatalyst cooperates with the transition metal catalyst are all unsettled problems. In this context, density functional theory (DFT) calculations were used to investigate the mechanism of the Ir/Pd co-catalyzed photocarboxylation of aromatic halides with CO_2.

In this study, all calculations were performed with the Gaussian 16 software [38]. The B3LYP functional [39,40] is used in the geometry optimization for all species. The effective core potential and the associated basis set of SDD [41] is used for Ir and Pd atoms, and the 6-31G(d, p) basis set is used for other atoms (including C, H, O, N, P, Br). Frequency analysis was performed at the same level

* Corresponding authors.
E-mail addresses: ice123wb@mail.ustc.edu.cn (B. Wang), yuhaizhu@ahu.edu.cn (H. Yu).

https://doi.org/10.1016/j.cclet.2020.09.045
1001-8417/

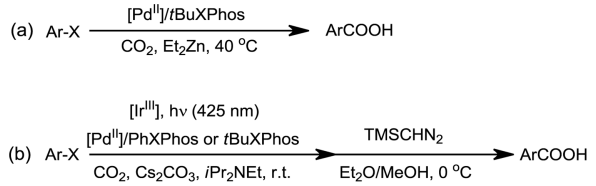

Scheme 1. Pd catalyzed dehalogenation-carboxylation of aromatic halides with CO_2 reported by Martin *et al.* (a); and Ir/Pd co-catalyzed carboxylation of aromatic halides reported by Iwasawa *et al.* (b).

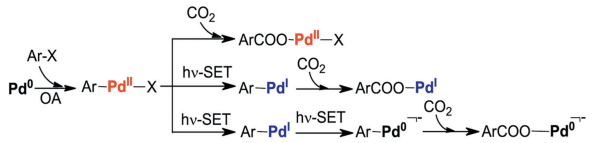

Scheme 2. The possible carboxylation pathways on $Pd^{0/I/II}$ species.

with geometry optimization to ensure the number of imaginary frequencies (1 for transition state and 0 for other species), and to obtain the thermal correction to Gibbs free energy. Single point energy calculations were carried out at a higher level of theory: B3LYP/def2-TZVP [42]. In all these calculations, the dispersion correction reported by Grimme and co-workers (*i.e.*, Grimme-D3BJ) was used [43], and *N,N*-dimethylacetamide was used as solvent (in accordance with Iwasawa's experiments [37], and with SMD model [44]). Natural bond orbital (NBO) [45] analysis was carried out at the same level with geometry optimization. The optimized structures were plotted by Cylview software [46].

Bromobenzene was chosen as the modeling reactant due to its structural simplicity and the high conversion efficiency. To this end, the dehalogenation and carboxylation of bromobenzene with CO_2 in the presence of Ir/Pd co-catalysts and PhXphos was used as model reaction (Eq. 1).

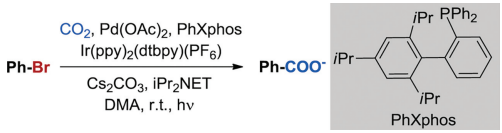

(1)

Our calculations start with the PhBr and PhXphos coordinated Pd^0 intermediate **I1** (Scheme 3). For clarity, **I1** was set as the energetic reference point. From **I1**, oxidation addition occurs easily *via* the typical three-membered ring transition state of **TS1** (barrier: 5.4 kcal/mol), and the relative energy of the formed **I2** is indicate that the oxidative addition is favored from both thermodynamic and kinetic aspect. Of note, **I2** was also verified by the experimental observations by Iwasawa and co-workers [37].

From **I2**, we first examined the possibility for its direct carboxylation with CO_2. As shown in Fig. 1, the approaching of CO_2 to **I2** generates the intermediates **I3**, from which the direct carboxylation occurs *via* the transition state **TS2** (Figs. 1 and 2).

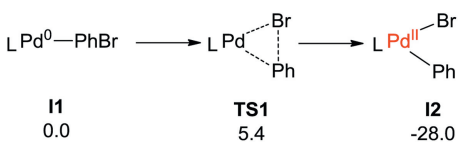

Scheme 3. Energy changes for the oxidative addition step (in kcal/mol, L= PhXphos).

The energy barrier for the transformation of **I3→TS2** is as high as 45.4 kcal/mol, presumably due to the high steric hindrance around the metal center (Fig. 2), the low nucleophilicity of aryl C1 atom (Fig. 1, with NPA charge of −0.081) and the Zwitterionic character of the transition state (NPA charge of O1/O2 atom is −0.648/−0.678) in **TS2**. Alternatively, a pre-dissociation of bromide could provide a vacant coordination site on the palladium center, making it possible to accommodate the dangling O2 atoms to reduce steric hindrance and avoid the formation of the Zwitterionic intermediates (**TS2** *vs.* **TS3** in Fig. 2). To this end, the energy barrier of the carboxylation step was decreased to 40.5 kcal/mol. Nevertheless, the energy demand of over 40 kcal/mol remain too high to occur under the experimental conditions. Therefore, the results herein indicate that the main difficulty in the Pd^{II} participated carboxylation lies in the low electron density of the aromatic group. In this context, we examined the possibility for a pre-reduction of the carboxylate precursor of **I2**.

I2 could be reduced by either the excited state of photocatalyst (*i.e.*, Ir^{III*}), or the reduced photocatalyst (Ir^{II}, *vide supra*) generated from the catalytic cycle of the photocatalyst. Therefore, the relative facility of the reductive and oxidative quenching of the photocatalyst was examined [47–50]. In oxidative quenching, Ir^{III*} is oxidized by **I2** to generate Ir^{IV} and **I6** (Scheme 4), while in the reductive quenching, Ir^{III*} is reduced by **Amine1** to generate **Amine2** and Ir^{II}. According to the calculation results, the reductive quenching is exergonic by 15.4 kcal/mol, and is more feasible than the oxidative quenching (endergonic by 2.6 kcal/mol). In addition, considering the existence of Cs_2CO_3, the removal of H^+ from **Amine2** (formed during the reductive quenching of photocatalyst) could occur easily to generate the radical $[iPrNEt(CMe_2)]^{\bullet}$ (**Amine3**). In this context, **Amine3** could possibly act as the electron donor to reduce **I2**. This process is exergonic by 1.7 kcal/mol (Scheme 4), and generates the cationic $[iPrNEt(CMe_2)]^+$ (**Amine4**) and the **I6**. By contrast, the reduction of **I2** with Ir^{II} (Ir^{II} + **I2**→Ir^{III} + **I6**) or Ir^{III*} mentioned above is endergonic by 6.4 and 2.6 kcal/mol (Scheme 4), and is thus less favorable.

From **I6**, the dissociation of Br^- occurs easily, generating a more stable, neutral intermediate **I7**. According to the calculation results, the released Br^- is unlikely to bind with the cationic **Amine4** to form contact ion pair or neutral complex (Scheme S1 in Supporting information). From **I7**, either a direct carboxylation (**I7→I8→TS4→I9**, Fig. 3) or a reduction [37]-carboxylation pathway (**I7→I11→I12→TS5→I10**) might occur (the reduction-dehalogenation pathway on **I7** was excluded due to the high energy demand for formation of the dianionic **I13**, Fig. 3).

In the first case, the approaching of CO_2 first generates the intermediate **I8**, and this step is endergonic by 12.3 kcal/mol. In **I8**, both the short Pd-C2 distance (2.19 Å in Fig. 4) and the Mayer bond order (0.44) indicate the pre-activation of CO_2. In the formed intermediate **I9**, the carboxylate product mainly coordinates with the palladium center *via* the terminal O2 atom (Fig. 4). The energy

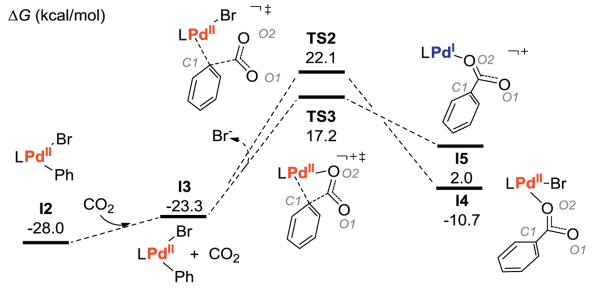

Fig. 1. Pd catalyzed reduction carboxylation (kcal/mol).

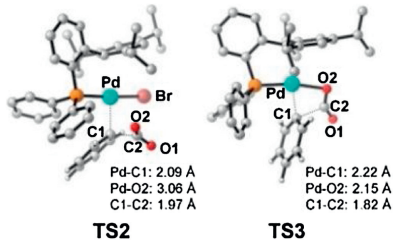

Fig. 2. The optimized geometries of **TS2** and **TS3**. H atoms are omitted.

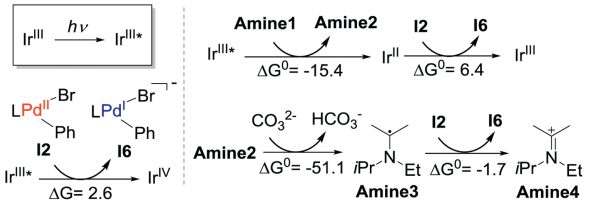

Scheme 4. The reduction of Pd^{II} intermediate **I2** (kcal/mol).

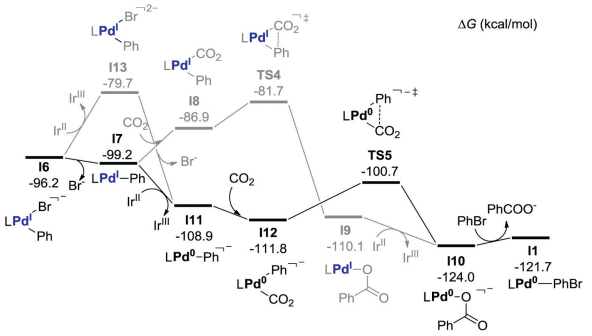

Fig. 3. Energy profiles for the possible carboxylation steps on **I6** (in kcal/mol).

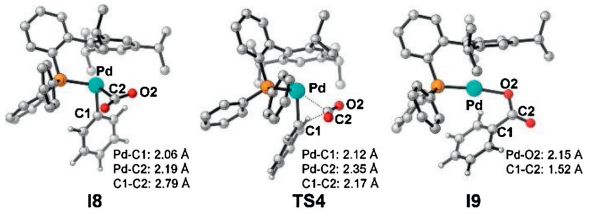

Fig. 4. The optimized geometries of **I8**, **TS4** and **I9**. H atoms are omitted.

barrier for the direct carboxylation on **I8** is 4.8 kcal/mol, and the relative Gibbs free energy of the formed **I9** is lower than **I8** by 23.2 kcal/mol. The remarkably lower energy barrier for the carboxylation step of **I8** than that of **I3** (5.2 *vs.* 45.4 kcal/mol) further evidences the importance of the enhanced nucleophilicity on the carboxylation step (NPA charge of the aryl C1 atom in **I8** and **I3** is −0.384 and −0.085). After that, the one electron reduction of **I9** could occur to generate a more stable, Pd^0 intermediate **I10**. Finally, the formed Pd^0 intermediate **I10** could undergo a ligand exchange to release the carboxylate product and regenerate **I1**.

In the second case, the reduction of **I7** with Ir^{II} is exergonic by 9.7 kcal/mol. Due to the high electron density on the Pd^0 center of **I11** (NPA charge on Pd is −0.540), the coordination of CO_2 occurs easily *via* an η^1-C coordination mode (exergonic by 2.9 kcal/mol), while the coordination of CO_2 by an end-on mode is unfavorable (Scheme S2 in Supporting information). The Pd-C1 distance in **I12** is 2.09 Å (Fig. 5), and its Mayer bond order of 0.71, indicating the formation of σ(Pd-C1) bond therein. Such intermediate is typical for the interaction of CO_2 with the electron rich metal complexes [51]. Thereafter, the C—C bond formation was achieved *via* the carboxylation transition state **TS5**, with a low energy barrier of 11.1 kcal/mol. The Pd^0 intermediate **I10** is then generated as the carboxylate product, and the subsequent transformation is the same as the aforementioned carboxylation-reduction pathway.

Comparing the different pathways in Figs. 1 and 3, the most feasible carboxylation pathway involves the cascade reduction of the Pd^{II} intermediate to Pd^0, associating with the release of bromide (**I2**→**I6**→**I7**→**I11**). Then the coordination of CO_2, carboxylation, and ligand exchange occurs to release the carboxylate product (**I11**→**I12**→**I10**→**I1**). In combination with the calculation results in Schemes 3 and 4, the rate determining step for the dehalogenation-carboxylation mechanism is the elementary carboxylation step, and the overall activation free energy barrier is 11.1 kcal/mol. The low energy barrier is in good agreement with the high efficiency of Iwasawa's reaction under room temperature [37]. More importantly, the easiness of the elementary carboxylation step was found to correlate with the nucleophilicity of the Pd precursor. According to the distortion-interaction analysis on the three key carboxylation transition states, *i.e.*, **TS3** (Pd^{II}), **TS4** (Pd^{I}) and **TS5** (Pd^0), the interaction energies between CO_2 and the other part in the target transition state decreases with reduced valence state of the Pd center (the interaction energy of **TS3**, **TS4**, **TS5** was −22.4, −36.4, −53.4 kcal/mol, respectively), demonstrating the stronger interaction between the reduced Pd complex and CO_2. The results verified the aforementioned proposal that the Pd complex with electron rich palladium center and aromatic groups are more prone to undergo a nucleophilic attack to CO_2. Nevertheless, due to the remarkably stronger interaction between CO_2 and Pd^0 complex in **TS5** (than that in **TS3** and **TS4**), CO_2 distorted significantly compared to the free state (Scheme S3 in Supporting information), and thus the distortion energy of **TS5** is significantly higher than **TS3** and **TS4** (49.5 *vs.* 40.6, 40.8 kcal/mol). To this end, the energy barrier of the transition state **TS4** with balanced the interaction and distortion energy is the lowest, while the weak interaction between the Pd^{II} center and CO_2 results in the highest energy barrier of **TS3**.

In this study, the mechanism for the dehalogenation-carboxylation of aryl halides recently reported by Iwasawa and co-workers were systematically studied by DFT calculations. The overall mechanism consists of oxidative addition of aryl halides, excitation and reductive quenching of the Ir^{III} photo-catalyst, successive reduction of Pd^{II} to Pd^{I} and Pd^0, removal of bromide, and carboxylation steps. The carboxylation with CO_2 is sensitive to the valence state of the palladium center, and thus the presence of reductant (*i.e.*, oxidized state of the photocatalyst Ir^{II} and the amine radical) is pivotal to the facility of the carboxylation step.

Declaration of competing interest

The authors report no declarations of interest.

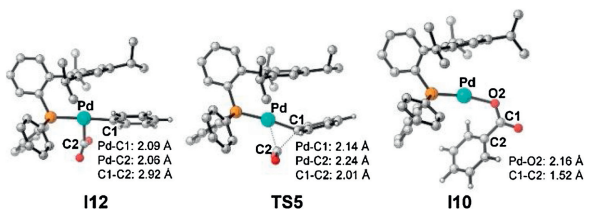

Fig. 5. The optimized geometries of **I12**, **TS5** and **I10**. H atoms are omitted.

Acknowledgments

We appreciate the financial support from the National Natural Science Foundation of China (Nos. 21672001, 51961135104) and the technical support of high-performance computing platform of Anhui University.

Appendix A. Supplementary data

Supplementary material related to this article can be found, in the online version, at doi:https://doi.org/10.1016/j.cclet.2020.09.045.

References

[1] K. Huang, C.L. Sun, Z.J. Shi, Chem. Soc. Rev. 40 (2011) 2435–2452.
[2] M. Cokoja, C. Bruckmeier, B. Rieger, et al., Angew. Chem. Int. Ed. 50 (2011) 8510–8537.
[3] Y. Tsuji, T. Fujihara, Chem. Commun. 48 (2012) 9956–9964.
[4] I. Omae, Coord. Chem. Rev. 256 (2012) 1384–1405.
[5] C. Maeda, Y. Miyazaki, T. Ema, Catal. Sci. Technol. 4 (2014) 1482–1497.
[6] C.S. Yeung, V.M. Dong, Top. Catal. 57 (2014) 1342–1350.
[7] D. Yu, S.P. Teong, Y. Zhang, Coord. Chem. Rev. 293–294 (2015) 279–291.
[8] Q. Liu, L. Wu, R. Jackstell, et al., Nat. Commun. 6 (2015) 5933.
[9] A. Tortajada, F. Juliá-Hernández, M. Börjesson, et al., Angew. Chem. Int. Ed. 57 (2018) 15948–15982.
[10] Y. Yang, J.W. Lee, Chem. Sci. 10 (2019) 3905–3926.
[11] L. Song, D.M. Fu, L. Chen, et al., Angew. Chem. Int. Ed 59 (2020) 21121–21128.
[12] X.W. Chen, L. Zhu, Y.Y. Gui, et al., J. Am. Chem. Soc. 141 (2019) 18825–18835.
[13] G. Courtois, L. Miginiac, J. Organomet. Chem. 69 (1974) 1–44.
[14] A.S. Hussey, J. Am. Chem. Soc. 73 (1951) 1364–1365.
[15] Y.J. Zhou, M. Xiao, S.J. Wang, et al., Chin. Chem. Lett. 24 (2013) 307–310.
[16] S. Xie, X. Gao, F. Zhou, et al., Chin. Chem. Lett. 31 (2020) 324–328.
[17] S.S. Yan, Q. Fu, L.L. Liao, et al., Coor. Chem. Rev. 374 (2018) 439–463.
[18] A. Tortajada, F. Juliá-Hernández, M. Börjesson, et al., Angew. Chem. Int. Ed. 57 (2018) 15948–15982.
[19] C.S. Yeung, Angew. Chem. Int. Ed. 58 (2019) 5492–5502.
[20] M. Shi, K.M. Nicholas, J. Am. Chem. Soc. 119 (1997) 5057–5058.
[21] J. Wu, N. Hazari, Chem. Commun. 47 (2010) 1069–1071.
[22] D.P. Hruszkewycz, J. Wu, N. Hazari, et al., J. Am. Chem. Soc. 133 (2011) 3280–3283.
[23] X. Feng, A. Sun, S. Zhang, et al., Org. Lett. 15 (2013) 108–111.
[24] C.S. Yeung, V.M. Dong, J. Am. Chem. Soc. 130 (2008) 7826–7827.
[25] H. Ochiai, M. Jang, K. Hirano, et al., Org. Lett. 10 (2008) 2681–2683.
[26] K. Ukai, M. Aoki, J. Takaya, et al., J. Am. Chem. Soc. 128 (2006) 8706–8707.
[27] J. Takaya, S. Tadami, K. Ukai, et al., Org. Lett. 10 (2008) 2697–2700.
[28] T. Ohishi, M. Nishiura, Z. Hou, Angew. Chem. Int. Ed. 47 (2008) 5792–5795.
[29] T. Ohishi, L. Zhang, M. Nishiura, et al., Angew. Chem. Int. Ed. 50 (2011) 8114–8117.
[30] W. Wang, G. Zhang, R. Lang, et al., Green Chem. 15 (2013) 635–640.
[31] H.A. Duong, P.B. Huleatt, Q.-W. Tan, et al., Org. Lett. 15 (2013) 4034–4037.
[32] Y. Makida, E. Marelli, A.M.Z. Slawin, et al., Chem. Commun. 50 (2014) 8010–8013.
[33] A. Correa, R. Martín, J. Am. Chem. Soc. 131 (2009) 15974–15975.
[34] T. Fujihara, K. Nogi, T. Xu, et al., J. Am. Chem. Soc. 134 (2012) 9106–9109.
[35] T. León, A. Correa, R. Martin, J. Am. Chem. Soc. 135 (2013) 1221–1224.
[36] H. Tran-Vu, O. Daugulis, ACS Catal. 3 (2013) 2417–2420.
[37] K. Shimomaki, K. Murata, R. Martin, et al., J. Am. Chem. Soc. 139 (2017) 9467–9470.
[38] M.J. Frisch, G.W. Trucks, H.B. Schlegel, et al., Gaussian 16, Revision A.01, Gaussian Inc., Wallingford CT, 2016.
[39] A.D. Becke, Phys. Rev. A 38 (1988) 3098–3100.
[40] C. Lee, W. Yang, R.G. Parr, Phys. Rev. B 37 (1988) 785–789.
[41] D. Andrae, U. Häußermann, M. Dolg, et al., Theor. Chim. Acta 77 (1990) 123–141.
[42] F. Weigend, R. Ahlrichs, Phys. Chem. Chem. Phys. 7 (2005) 3297–3305.
[43] S. Grimme, S.L. Ehrlich, J. Comput. Chem. 32 (2011) 1456–1465.
[44] A.V. Marenich, C.J. Cramer, D.G. Truhlar, J. Phys. Chem. B 113 (2009) 6378–6396.
[45] A.E. Reed, R.B. Weinstock, F. Weinhold, J. Chem. Phys. 83 (1985) 735–746.
[46] C.Y. Legault, CYLview, Version 1.0B, (2009) , http://www.cylview.org/.
[47] M.H. Shaw, J. Twilton, D.W.C. MacMillan, J. Org. Chem. 81 (2016) 6898–6926.
[48] M.D. Levin, S. Kim, F.D. Toste, ACS Cent. Sci. 2 (2016) 293–301.
[49] L. Buzzetti, G.E.M. Crisenza, P. Melchiorre, Angew. Chem. Int. Ed. 58 (2019) 3730–3747.
[50] J.D. Slinker, A.A. Gorodetsky, M.S. Lowry, et al., J. Am. Chem. Soc. 126 (2004) 2763–2767.
[51] D.H. Gibson, Coord. Chem. Rev. 185–186 (1999) 335–355.